ICES Journal of Marine Science

ICES Journal of Marine Science (2021), 78(3), 782–796. doi:10.1093/icesjms/fsaa242

Review Article

Ex situ and *in situ* target strength measurements of European anchovy in the Bay of Biscay

B Sobradillo [1]*, G Boyra [1], I Pérez-Arjona[2], U Martinez[1], and V Espinosa[2]

[1]*Marine Division, Azti-Tecnalia, Herrera kaia, portualdea z/g, Pasaia 20110, Spain*
[2]*Institut d'Investigació per a la Gestió Integrada de Zones Costaneres, Universitat Politècnica de València, C/Paranimf 1, Grau de Gandía, València 46730, Spain*

**Corresponding author: tel: +34 652 714 457; e-mail: beasobradillo@gmail.com.*

Sobradillo, B, Boyra, G, Pérez-Arjona, I, Martinez, U, and Espinosa, V *Ex situ* and *in situ* target strength measurements of European anchovy in the Bay of Biscay. – ICES Journal of Marine Science, 78: 782–796.

Received 20 June 2020; revised 5 December 2020; accepted 7 December 2020; advance access publication 23 January 2021.

This study measures the dorsal aspect target strength (*TS*; dB re 1 m^2) and *TS*–length (standard length, SL; cm) relationships for European anchovy, attained both *ex situ* and *in situ* in two different seasons across 7 years in the Bay of Biscay. The measurements were made at three frequently used acoustic frequencies (38, 120, and 200 kHz). A backscattering model for physostome fish was utilized to help interpret the results. The obtained experimental mean *TS* for anchovies with an SL of 3.5–19.5 cm was −44.6 (±2.3), −46.9 (±3), and −48.4 (±2.7) dB at 38, 120, and 200 kHz, respectively, yielding b_{20} values of −66.4, −68.7, and −70.4 dB, respectively. The results were consistent across seasons and between *in situ* and *ex situ* conditions, presenting *TS*–length relationships with statistically significant slopes (*p*-values <0.05) for all frequencies. This research represents part of a series of efforts planned to obtain a comprehensive *TS* vs. length and depth relationship to update the acoustic assessment methodology of European anchovy in the Bay of Biscay.

Keywords: *Engraulis encrasicolus*, *ex situ*, *in situ*, method of fundamental solutions, target strength

Introduction

European anchovy (*Engraulis encrasicolus*; Linnaeus, 1758) is one of the main commercial species in the Bay of Biscay, supporting profitable fisheries for both the Spanish and French fleets. Stock assessment of this resource is based on the so-called catch-Bayesian biomass-based model (CBBM) (Ibaibarriaga *et al.*, 2008; ICES, 2015), which depends on the internationally coordinated scientific advice. This advice is based in an abundance index of the adult stock abundance, derived from a combination of commercial and fisheries independent information. The scientific surveys that contribute to the CBBM are BIOMAN (Massé *et al.*, 2018); based on the daily egg production method in spring; and two acoustic-trawl surveys, PELGAS (Massé *et al.*, 2018) in the spring and JUVENA (Boyra *et al.*, 2013) in autumn. These surveys' methodologies are discussed and evaluated annually at the International Council for the Exploration of the Sea Working Group of Acoustics and Eggs (ICES WGACEGG) and the results are synthetized at the ICES Working Group on Southern Horse Mackerel, Anchovy and Sardine (ICES, 2017) to produce the CBBM index.

Acoustic surveys are considered effective methods for quantifying the distribution and abundance of many pelagic marine fauna (Simmonds and Maclennan, 2005). In most cases the echo-integration technique is used to estimate fish density (MacLennan *et al.*, 1990), necessitating information regarding the dorsal aspect target strength (*TS*; dB re 1 m^2)

(Maclennan *et al.*, 2002) of the fish that contributes to the received signal (Jech and Horne, 2001). The *TS* is a measure of the proportion of the incident intensity that is backscattered by the target (Maclennan *et al.*, 2002). To translate acoustic density measurements into biologically more meaningful measures, such as biomass or abundance, the log-linear relationship between the standard length (SL; cm) of the fish and the backscattered acoustic energy is commonly used. This *TS* to length (*TS*–L) equation can be expressed as:

$$TS = a \log_{10}(\mathrm{SL}) + b, \quad (1)$$

where the slope, *a*, and the intercept, *b*, are generally assumed to be species-specific constants. In the case of physostomous fish such as anchovy, *a* is normally close to 20 (Love, 1977; Foote, 1980) and (1) is often replaced by:

$$TS = 20 \log_{10}(\mathrm{SL}) + b_{20}. \quad (2)$$

The acoustic surveys that are currently used to estimate anchovy biomass in the Bay of Biscay utilise different b_{20} values at 38 kHz: the French survey PELGAS uses −71.2 dB, originally obtained from 19 to 35 cm herring *Clupea harengus* (ICES, 1982), while the Spanish surveys JUVENA and PELACUS use −72.6 dB from 8 to 32 cm herrings (Degnbol *et al.*, 1985). The lack of unique and *ad hoc* *TS*–length relationship for Bay of Biscay anchovy presents an obstacle for the development of an absolute index of abundance for this species. This has been acknowledged by ICES WGACEGG, with the attainment of a common *TS*–length relationship for the region deemed one of the key objectives of the working group (ICES, 2013).

Generally, *in situ* *TS* measurements are assumed to deliver accurate results when collected with concurrent reliable biological samples and tilt angle information (Torgersen and Kaartvedt, 2001; Madirolas *et al.*, 2016; Zare *et al.*, 2017). However, measuring the *TS* of fish in their natural environment may be accompanied by difficulties that result in biased *TS* values. In particular, during the daytime small pelagic fish such as European anchovy aggregate in schools that are too densely packed to resolve individual targets (Sawada *et al.*, 2009). Nevertheless, various strategies exist to overcome this problem. One mitigation tactic is to lower transducers closer to the fish targets, thus reducing the sampling volume (Ona, 2003; Kang *et al.*, 2009; Sawada *et al.*, 2009; Murase *et al.*, 2011; Fernandes *et al.*, 2016). In the Bay of Biscay, a variant of this technique has been applied to estimate the *TS* of anchovy (Doray *et al.*, 2016), but the methodology stimulated a change in fish behaviour that seemed to positively bias the mean *TS* values. Other strategies involve working at night, when most species disperse and migrate near the surface (Glass, 2000). These are most useful when a study area is dominated by the target species (Foote *et al.*, 1987; Barange *et al.*, 1996; Peltonen and Balk, 2005; Zhao *et al.*, 2008) but might prove problematic where there are numerous fish species or in the presence of high abundances of plankton.

An alternative strategy is to conduct *ex situ* experiments (Kang and Hwang, 2003; Kang *et al.*, 2009), providing greater control over density and ensuring the isolation of the target species. However, *ex situ* experiments pose some concerns such as potentially altering the behaviour of the targets (and hence potentially biasing the mean *TS* values) or the close proximity of the targets to the transducers, which may cause short-range problems [i.e. *TS* dependence with distance related to measurements performed inside the near field of the transducer (Simmonds and Maclennan, 2005; Foote, 2014; Chu and Eastland, 2015; Pérez-Arjona *et al.*, 2018), or the extended size of fish that produces an uncertainty in the position inside the beam measured by split-beam echosounders (Kieser *et al.*, 2000)]. To gain insights regarding the influence of behaviour on *TS*, modelling techniques (Fujino *et al.*, 2009) have often been used in combination with *ex situ* *TS* measurements (Henderson and Horne, 2007; Sawada *et al.*, 2011).

The objective of this work is to measure the *TS* values and model *TS*–length relationships for European anchovy at 38, 120, and 200 kHz frequencies, using acoustic data collected both *in situ* and *ex situ*. A reduction in potential multiple target bias was attempted by working during the night and applying a high-density filter (Gauthier and Rose, 2001) to the *in situ*-measured data as well as controlling the influence of the different sampling volumes related to the pulse durations used at the different *ex situ* experiments. In addition, an *ad hoc* calibration experiment was conducted to correct the possible bias derived from the short range of some of the *ex situ* measurements that were done in the transition range between near and far field. Finally, a backscattering model based on the method of fundamental solutions (MFS) (Fairweather *et al.*, 2003; Pérez-Arjona *et al.*, 2018, 2020a) for physostomous fish, simulating the swimbladder as two-chambered prolate spheroids (Andreeva, 1974; Weston, 1966; Love, 1978; Furusawa, 1988; Ye, 1997) plus the backbone, was utilised to help interpret the empirical results. Most of the numerical methods considered for the simulation of *TS* values are solely valid when estimating *TS* in the far field of both the emitting transducer and the scatterer (fish) (Jech *et al.*, 2015). Only the finite element method (FEM) (Lilja *et al.*, 2004) and the boundary-element method (BEM) (Foote and Francis, 2002) provide alternatives at arbitrary close distances, but they (especially FEM) have a high and perhaps even unaffordable computational cost. The MFS is a meshless method that has proved to be useful in estimating the measurable *TS* of fish and the contributions of the different inner structures of fish to *TS*. It has similar or even greater accuracy than FEM or BEM (Godinho *et al.*, 2012), yet with reduced computational costs, which is a consideration that is especially important when examining fish models with additional fish structures to a swim bladder (e.g. a fish backbone) (Pérez-Arjona *et al.*, 2018).

Material and methods

In situ data collection

Acoustic-trawl data were collected from 2010 to 2017 via two scientific surveys in the Bay of Biscay at two different times of year (Figure 1). JUVENA (Boyra *et al.*, 2013) was conducted in September and mainly focused on the juvenile component of the anchovy population, while BIOMAN (Santos *et al.*, 2016) was undertaken in May (during the peak of the spawning season) and examined the adult component. Two scientific research vessels were used in each survey: RV "Ramón Margalef" (RM, hereafter) and RV "Emma Bardán" (EB, hereafter). Both collected continuous acoustic data using a Simrad EK60 scientific echosounder, with split-beam transducers of 38 kHz (ES38B-7), 120 kHz (ES120-7C), and 200 kHz (200-7C). The echosounders were calibrated at least once a year, typically at the beginning of the survey following standard procedures (Demer *et al.*, 2015), with

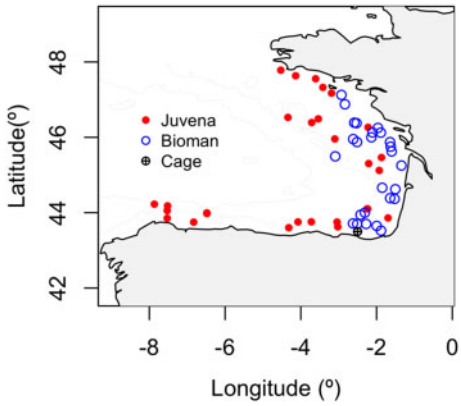

Figure 1. Area of study in the Bay of Biscay, with the locations where the *TS* measurements were performed, distinguishing the fishing trawls conducted for the *in situ* measurements in both surveys and the location of the cage for the *ex situ* ones.

intercalibration exercises carried out each year between the two vessels following a standard methodology (Simmonds and Maclennan, 2005). The most relevant calibration parameters of the *in situ* measurements are described in Supplementary Table S1.

Ground truth trawl hauls were performed based on the interpretation of the echograms, aiming to identify fish species and to determine their size distribution across the whole area of study. Both vessels performed trawl hauls during JUVENA, but only EB performed trawl hauls during BIOMAN due to the regular activities that take place on the RM in association with the daily egg production method. Trawl samples were obtained using a Gloria HOD 352 pelagic trawl of 15-m vertical opening, with a 10-mm mesh size (bar length) at the cod end. Fishing trawls were performed during the day and the night, between 5- and 300-m depth and at a mean speed of 4 knots. Acoustic data recorded during trawl hauls with predominance (>85%) of anchovy in the catch were selected for *TS* analysis (Supplementary Table S2). The typical recording range was 200 m, yielding 2–3 pings per second. Lengths were obtained from a random sample of >50 individuals of each haul and measured to 0.5-cm SL classes onboard the research vessel.

Ex situ data collection

Ex situ TS measurements were obtained from two sets of anchovy individuals, captured in December 2011 (set 1) and July 2013 (set 2) in the Bay of Biscay. Both were captured by the purse seiner Itsas Lagunak and transported in live bait fishing tanks onboard the vessel. The first set comprised 120 anchovies that were kept in water tanks (1 m depth × 3 m diameter) in the Aquaculture School of Mutriku for eight months before being moved to the sea culture cage at the mouth of Mutriku harbour (Gipuzkoa, Spain; 43°18′N, 02°22′W) (Figure 1). The cage was cylindrical with ∼8 m depth and 16 m diameter and a mesh size of 0.4 cm. The second set consisted of ∼5000 anchovies and was transported directly from the purse seiner tanks to the harbour cage. After being moved to the cage, anchovies were left at least two days to settle before the experiments commenced. Unfortunately, after dropping the second set of anchovies to the cage, we noticed that it was contaminated by number with ∼2% of horse mackerel. A diver visually inspected the cage periodically to maintain, feed and monitor the fish. Two groups of measurements (N1, N2) were carried out using the first set of anchovies and another (N3) using the second one. At the end of each set of measurements, 50 specimens were weighed and measured for SL.

TS measurements were made using a three-frequency (38, 120, and 200 kHz) Simrad EK60 split-beam scientific echosounder system, installed on a floating 0.6 m × 0.6 m platform ∼20 cm below the sea surface. The floating platform was placed about halfway (∼4 m) between the centre and the border of the cage (Figure 2a). The platform was connected to a logistics boat that housed the ancillary electronic equipment and the 12-V batteries used as the power source. Day- and night-time data were registered during the study, but following a preliminary inspection of the data, only night experiments were used in the analysis. Daytime data yielded significantly higher *TS* values, probably owing to the greater packing densities reported by the diver and hence likely subjected to a higher probability of detecting unresolved multiple echoes.

Measurements at the cage were performed using different pulse durations (64, 128, 256, and 512 μs) to check whether the values obtained varied at increasing sampling volumes (i.e. decreasing vertical resolutions) due to the greater failure probability of the single target discrimination algorithm for larger volumes (see below). Calibrations were made following standard procedures (Demer *et al.*, 2015) and were repeated for all pulse durations and power settings (Table 1).

In addition to the regular calibration at 4 m range, an additional calibration experiment was conducted to determine and correct the bias effect of working at distances where the far field condition of the corresponding transducer was not achieved (see below).

Near-to-far field calibration experiment

Due to the limited cage dimensions (Figure 2), some of the acoustical measurements were done closer than the far field distance of the 38-kHz transducer, which posed some initial concerns about the validity of these measurements. Depending on the distance from the transducer face, three main regions can be distinguished: the near field, the far field and a near-to-far transition field (Figure 2). The *near field* is the region of distances closer than R_C, the critical range or Fresnel distance, which for the corresponding flat piston transducer is defined as $R_C = a^2/\lambda$, being a the transducer radius and λ its operative wavelength (Medwin and Clay, 1998; Foote, 2014). Inside the near field (i.e. at distances less than 1.14, 0.46, and 0.33 m, respectively, for the 38, 120, and 200 kHz transducers used in this work; radius of each transducer shown in Table 1) the amplitude oscillates with distance (Figure 2) and quantitative acoustic measures are problematic. Immediately beyond R_C lies the *near-to-far transition field*, where the amplitude does not oscillate with distance and the spreading beam directivity pattern is stable, with the on-axis amplitude decreasing monotonously but not yet following spherical spreading. Finally, beyond the transition zone is the *far field*, where the amplitude decreases spherically with range. The far field starts somewhere between two to four times R_C (depending on the maximum deviation allowed from spherical spreading (Foote, 2014)). In this work, taking a rather conservative assumption ($4R_C$), the far field condition was accomplished at different distances for each frequency: 4.55 m at 38 kHz, 1.85 m at 120 kHz,

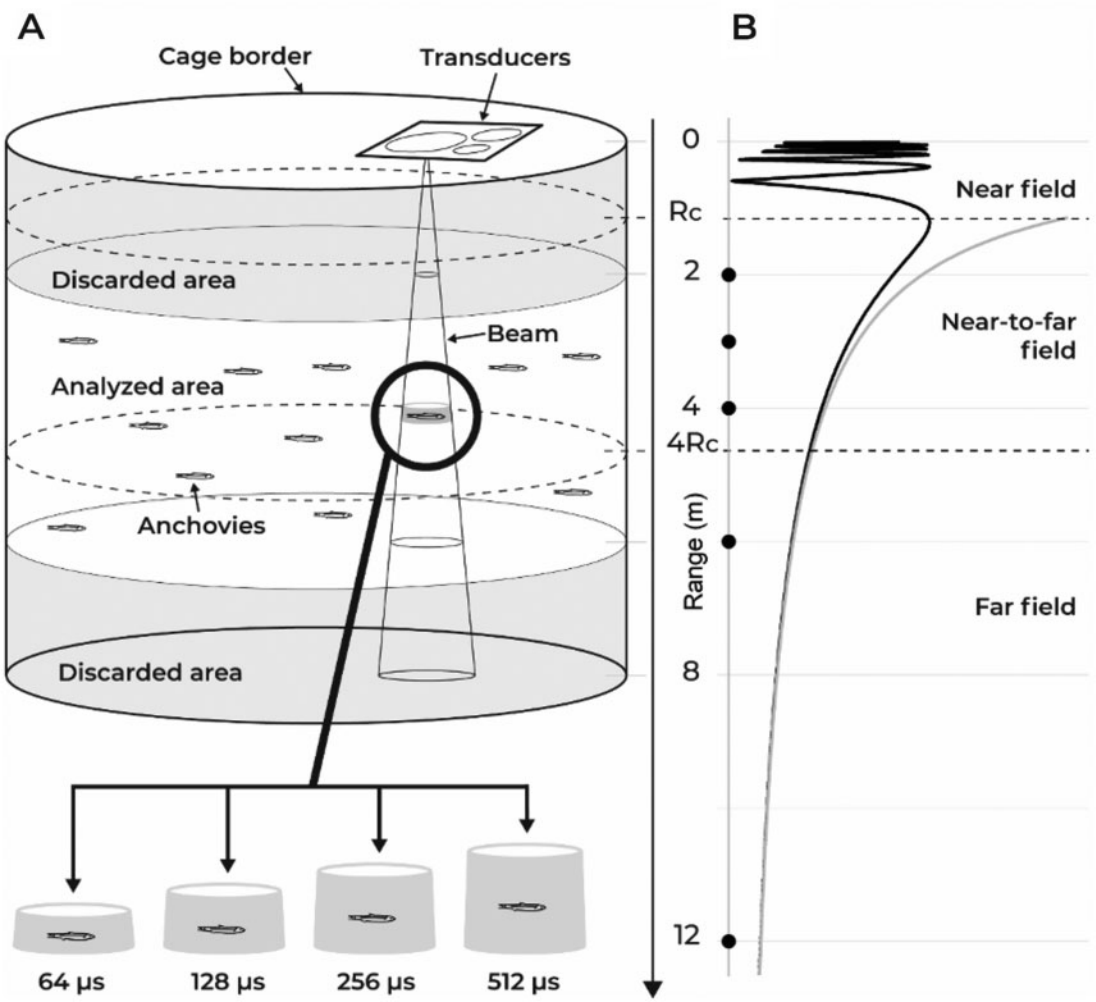

Figure 2. (a) Scheme of the experimental set up in the cage. Transducers were installed in a floating platform near the surface pointing downwards towards the scattered anchovies. Different regions are highlighted with reference to the different acoustic fields (near, near-to-far and far field; shown in B) of the used 38 kHz transducer. The dashed lines mark the critical ranges (Rc and 4Rc) that divide the three regions. The *TS* analysis was done using decreasing pulse durations to achieve increasing sampling resolution (note that neither anchovies nor sampling volumes are at proportional scale). Targets from the grey areas (i.e. depth <2 and >6 m) were not used for analysis. (b) Theoretical range-dependence of the pressure wave of a circular piston simulating the geometry of a Simrad ES38B transducer (see the text for details), showing both the exact solution (black line) and the far field aproximation (i.e. spherical decay, grey line). The different ranges at which the sphere was calibrated during the near-to-far field calibration experiment are also marked (black circles). The calibration values at each range obtained in this experiment were used to correct the anchovy *TS* measurements of the corresponding range in the cage.

Table 1. Calibration settings of the *ex situ* data, performed at 4 m from the transducer.

Year	Experiment code	Frequency (kHz)	Transducer radius (m)	Pulse duration (µs)	Power (W)	Gain (dB)	S_a correction (dB)
2012	N1	38	0.21	256	800	23.62	−0.66
		120	0.08	256	200	23.55	−0.59
		200	0.05	256	180	25.74	−0.44
2012	N2	38	0.21	256	800	23.51	−0.65
		120	0.08	64	200	25.23	−0.58
		200	0.05	64	180	24.74	−0.67
2013	N3	38	0.21	512	800	25.4	−0.75
		120	0.08	256	200	26.63	−0.61
		200	0.05	128	180	26.07	−0.76

Note that the 200-kHz gain values differ from the observed increasing trend with time because there were two different 200-kHz transducers used.

and 1.33 m at 200 kHz. Therefore, as only targets from 2 to 6 m depth were analysed (Figure 2), only those performed at 38 kHz were susceptible to be biased by this effect. Moreover, since the considered measuring distances were greater than R_C (1.14 m at 38 kHz) but smaller than *4Rc*, measurements followed a stable pattern. It is for this reason that the corrections can be applied not only at the calibration points but also interpolated to intermediate distances.

To test the validity of these data and, when necessary, to obtain an extra depth-dependent gain correction, an *ad hoc* calibration experiment was carried out, in which the *TS* of a reference target (a tungsten carbide sphere of 38.1 mm diameter) was measured on axis at different distances from a 38 kHz transducer (2, 3, 4, 6, and 12 m), i.e. covering distances from the near-to-far to the far field (Figure 2b). The *TS* of the sphere was first measured at 12 m (i.e. well beyond the far field range and, thus, where the target measurements were expected to be free from bias caused by range) and then at all the other ranges. We simulated the pressure waves emitted by a 38 kHz transducer using the analytical solution of the pressure radiation of a circular flat piston (Kinsler *et al.*, 1999, pp. 181–185) at different ranges, to visualize (Figure 2b) and help interpret the results of the near-to-far field experiment.

Data processing

Target selection

In situ data

To separate swimbladdered fish from fluid-like organisms or macro-zooplankton, a bi-frequency algorithm (Ballón *et al.*, 2011; Lezama-Ochoa *et al.*, 2011) was used on the *in situ* experiments, based on the differences in mean volume backscattering strength (S_v, dB re 1 m^2/m^3) at 38 and 120 kHz. It was possible to use this algorithm because of the high percentage of beam overlap within the *in situ* measurements ranging from 60 to 86% (see here an interactive application illustrating the beam overlap calculations). A binary matrix was created from the data selected by the algorithm and was applied as a mask to the three frequencies of the study using Echoview Software Pty Ltd, 2013, version 5.2 (Echoview Software, 2013). All the echograms were visually inspected to check the correct performance of the algorithm (Figure 3). The *TS* values were then derived from the selected echoes using a single target detection algorithm (Soule, 1997; Ona and Barange, 1999), the values of which are presented in Table 2.

Ex situ data

Due to the short depth range available in the experimental cage, the overlapping volume between the 38- and 120-kHz frequencies (42%) was not enough to apply the bi-frequency algorithm (link to the interactive beam overlap illustration). Therefore, it could not be used with the *ex situ* data. Instead, echograms were manually scrutinized to isolate anchovies from unwanted signals based on the intensity and the length of the echo-traces. There were two clearly distinguishable types of traces: intense ($TS > -60$ dB) and short (<4 consecutive pings, representing typical swimming velocities of small pelagic fish between 7 and 20 cm/s in most cases), attributed to anchovy, and less intense (<−60 dB) and long (typically between 20 and 100 pings, representing velocities between 0.2 and 2 cm/s) were attributed to slow-swimming (presumably planktonic) scatterers.

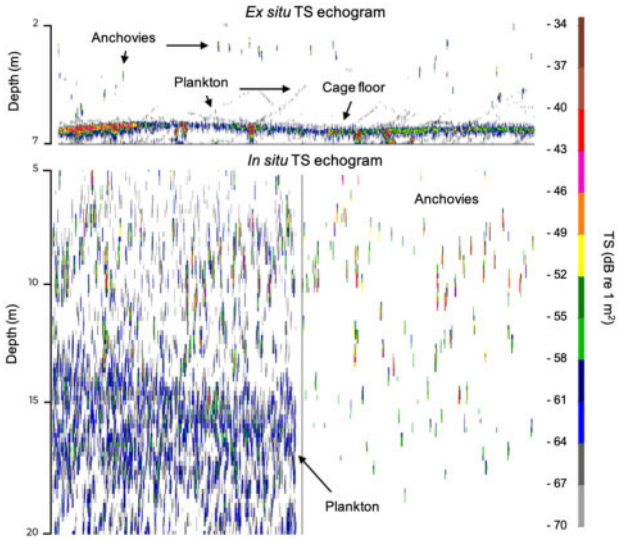

Figure 3. Top panel: example of 38 kHz *TS* echogram showing 10 min of one of the *ex situ* experiments (N1) targeting ∼10 cm anchovies at 256 μs pulse duration and −70 dB threshold. Anchovies and plankton are easily distinguished by intensity and length of the echotraces. Bottom panels: example of 38 kHz *TS* echogram showing 2.5 min of the 165 037 *in situ* haul targeting ∼12 cm anchovies at 1024 μs pulse duration and −70 dB threshold. The left side shows the raw *TS* echogram where the anchovies (yellow-red echoes) are surrounded by a plankton layer (grey-blue echoes); and the right side shows the same 2.5 min of acoustic data at the same threshold but after the plankton filtering process, where only fish echoes remain (see the text for details).

Table 2. Parameters used in the single target detection algorithm.

	Units	*In situ*	*Ex situ*
TS threshold	dB	−70	−70
Filter angles (major/minor)	Degrees	3.5	3.5
Min. pulse length	ms	0.7	0.7
Max. pulse length	ms	1.5	1.5
Max. beam compensation	dB	6	6
Max. angle SD (minor/major)	Degrees	0.6	0.2

Multiple targets

To prevent the inclusion of unwanted multiple targets, two different procedures were followed depending on the type of data collected.

In situ

To reduce the multiple target bias associated with the *in situ* data, a high-density filter (Gauthier and Rose, 2001) was applied, for which the density threshold was empirically determined. The echogram of each haul was gridded in cells with a horizontal size of 5 pings (1 ping ≈ 1.8 m) and a vertical length of 5 m. The total number of fish per acoustic reverberation volume (N_v) (Sawada *et al.*, 1993; Ona and Barange, 1999) was then plotted against the number of single targets per sample volume (T_v) in each cell. As in previous studies (Boyra *et al.*, 2018, 2019), the maximum of T_v on N_v was used to determine the target density at which multiple target echoes are likely to be produced. However, in this study, rather than having a maximum, the T_v values were found to

monotonously increase for small values of N_v until reaching stabilization at N_v values close to 1. This may have been due to the lower packing density observed, related to the typical dispersed night-time distribution of anchovy. The *in situ* data set was subsequently limited to cells with N_v values below 1. After filtering the high-density areas, a final quality check consisted on removing the hauls that presented either two similarly pronounced modes or fewer than five targets.

Ex situ

Measurements at the cage were performed at different pulse durations (Figure 2a). If the proximity between anchovies in the cage caused unresolved multiple targets, the probability of occurrence (and hence the mean *TS*) was expected to increase at higher pulse durations. In addition, the single target detection performance was tested for values of maximum standard phase deviation between 0.2° and 0.9° (Ona and Barange, 1999).

Table 3 summarizes the different procedures performed during the *in situ* and *ex situ* data collection and processing.

TS–length and TS–depth relationships

Averaged *TS* values from each haul or cage experiment were plotted against mean length in the logarithmic scale to determine the *TS*–L relationship from (1) and (2) at the three frequencies. Linear regression models were fit at each frequency, providing probability values and coefficients of determination to measure the goodness of the relationships (p-values <0.05 were considered statistically significant). Obtained *TS*–length relationships were also compared with those predicted by the MFS model (see below), analysing the agreement between empirical and modelled data in terms of the pairs of mean and standard deviation of fish tilt angle used in the model as a proxy of anchovy behaviour.

Finally, *TS* vs. length and depth relationships were investigated by means of linear models. To avoid the violation of independence of the explanatory variables we studied possible collinearity between depth and length.

Acoustic scattering model

To interpret the measured *TS* values, a numerical model of acoustic scattering for European anchovy was applied using the MFS (Fairweather *et al.*, 2003; Pérez-Arjona *et al.*, 2018). Anchovy is a physostomous fish with a dual-chambered swimbladder, which the simulation simplified as two-chambered prolate spheroids (Andreeva, 1974; Weston, 1966; Love, 1978; Furusawa, 1988; Ye, 1997) (PS_1 and PS_2). The major axis of the PS_1 was considered orthogonal with respect to the incident acoustic pulse when fish was swimming horizontally and the major axis of PS_2 was tilted α with respect to the major axis of PS_1 (Figure 4). The model also considered the backbone's contribution, which was expected to attenuate the swimbladder signal and/or modify the far-field distance achievement, while discarding the flesh's contribution which is usually less significant for swimming directions close to the horizontal (Pérez-Arjona *et al.*, 2020b). The prolate spheroids' dimensions and tilt angle (Figure 4) were based on soft X-ray images (IntechForView CR system).

Twelve good quality, freshly thawed individuals were radiographed and their swimbladder condition was visually examined from the digitized images. Individuals with ruptured or disfigured bladders were discarded, with the four individuals that appeared to be undamaged ultimately used for the morphological measurements (Figure 4).

Calculations were carried out for mean SL = 10.5 cm, with corresponding PS_1 and PS_2 dimensions given by length (semi-major axes, $a_1 = 0.625$ cm and $a_2 = 0.5$ cm), height (semi-minor axes, $b_1 = 0.2$ cm and $b_2 = 0.2$ cm), width (semi-minor axes $c_1 = b_1$ and $c_2 = b_2$), and relative angle $\beta = 12$ degrees, being β the tilt angle with respect to the fish body axis (Figure 5). The two-chambered swimbladder was deemed a pressure-release surface. The fish backbone was modelled as a fluid-filled ($\rho = 1100\,\mathrm{kg/m^3}$, $c = 2270$ m/s) (Gorska *et al.*, 2005; Pérez-Arjona *et al.*, 2018) straight cylinder (length = 9 cm and radius = 1 mm) with smooth edges surrounded by a homogeneous host medium (seawater with acoustical properties $\rho = 1026\,\mathrm{kg/m^3}$, $c = 1490$ m/s).

MFS was used to solve the three-dimensional Helmholtz equation in the frequency domain (Fairweather *et al.*, 2003).

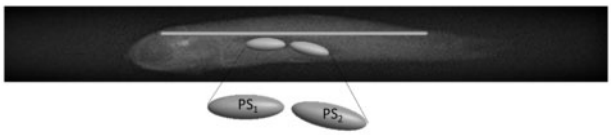

Figure 4. Lateral radiograph of a specimen of *Engraulis encrasicolus* showing the two connected swimbladder chambers (PS1 and PS2) and the backbone. Fish length = 10.1 cm, fish height = 1.04 cm.

Table 3. Methodological differences between the *in situ* and *ex situ* data collection and processing.

	In situ	*Ex situ*
Sampling period	2010–2017	2012–2013
Season	Autumn, spring	Winter
Age	Juvenile (5.8–16.3 cm) Adult (10–15.94 cm)	Juvenile (10.1–10.9 cm)
Survey metdodology	Daily Egg Production Metdod and acoustics	Acoustics
Data processing		
Target selection	Bi-frequency algoritdm (Ballón *et al.*, 2011; Lezama-Ochoa *et al.*, 2011)	Manual selection of anchovy echo signals
Single target detection algoritdm parameters: standard deviation of minor/major axis	0.6°	0.2°
Extra multiple targets filtering	High-density filter (Gautdier and Rose, 2001)	Measurements at different sampling volumes (pulse durations)
Data collection		

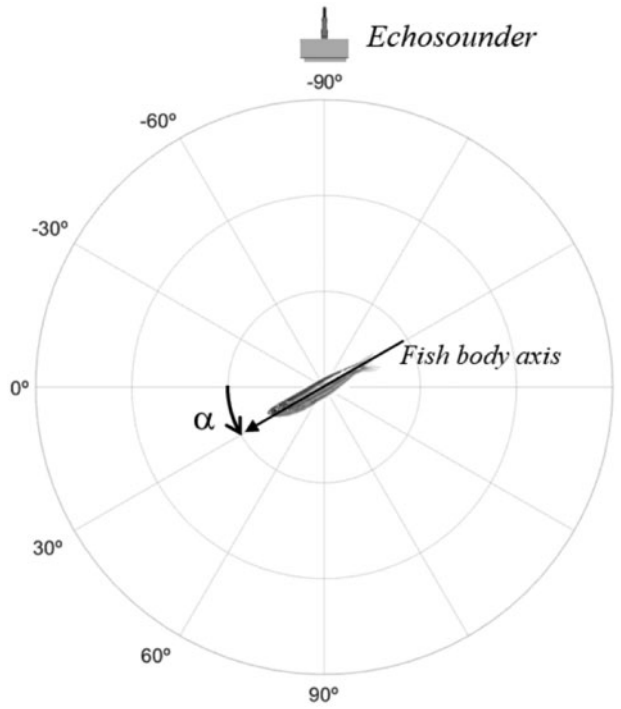

Figure 5. Scheme of the *TS* directivity *TS*(α), being α the tilt angle of fish body axis with respect to the horizontal. The emitting and receiving echosounder position are fixed and depicted in the diagram. The echosounder's emitted beam axis is orthogonal to the fish body axis for $\alpha = 0^\circ$.

For the 3D case, assuming a point source placed within the propagation domain, at point $\boldsymbol{x}_0$, it is possible to establish fundamental solutions of the Helmholtz equation G, for the sound pressure, and H, for the particle velocity, at a point x, which can be written respectively as:

$$G^{3D}(\boldsymbol{x}, \boldsymbol{x}_0, k) = \frac{e^{-ikr}}{r}, \tag{3}$$

$$H^{3D}(\boldsymbol{x}, \boldsymbol{x}_0, k, \vec{n}) = \frac{1}{-i\rho\omega}\frac{(-ikr-1)e^{-ikr}}{r^2}\frac{\partial r}{\partial \vec{n}}. \tag{4}$$

In these equations, r corresponds to the distance between the source point and the domain point, given; $\vec{n}$ represents the direction along which the particle velocity is calculated, $k{=}\omega/c$ the wave number, $\omega{=}2\pi f$ the angular frequency, f the frequency and c the sound propagation velocity within the acoustic medium and the medium density. The basic principle of the MFS (Fairweather *et al.*, 2003; Pérez-Arjona *et al.*, 2018) is that the sound field in a homogeneous region can be simulated by the linear superposition of the effects of a number of virtual sources, each one with its own amplitude. To define the formulation of this problem, let us first consider three sets of virtual sources located: the first within the swimbladder, with NS1 sources; the second within the spine, with NS2 sources; the third in the water, distributed around the spine, also with NS2 sources. The first two sets will allow the simulation of the sound field in the host medium, which, in that case, can be written as

$$p(\boldsymbol{x}, k)_{\Omega_1} = \sum_{j=1}^{NS1} P_j G^{3D}(\boldsymbol{x}, \boldsymbol{x_{1,j}}, k_1) + \sum_{j=1}^{NS2} Q_j G^{3D}(\boldsymbol{x}, \boldsymbol{x_{2,j}}, k_1) + p_{inc}(\boldsymbol{x}, \boldsymbol{x}_{source}, k_1) \text{ for } \boldsymbol{x} \text{ in } \Omega_1, \tag{5}$$

while within the spine the acoustic pressure is given as

$$p(\boldsymbol{x}, k_2)_{\Omega_2} = \sum_{j=1}^{NS3} R_j G^{3D}(\boldsymbol{x}, \boldsymbol{x_{3,j}}, k_2) \text{ for } \boldsymbol{x} \text{ in } \Omega_2. \tag{6}$$

In (2) and (3), P_j, Q_j, and R_j are unknown amplitudes of the virtual sources, $p_{inc}(\boldsymbol{x}, \boldsymbol{x}_{source}, k)$ represents the incident field generated by a source located at x_{source} and k_1 and k_2 represent the wavenumber in the host medium (water) and in the spine. To determine the relevant amplitudes, a system of equations must be established by imposing the necessary interface and boundary conditions. A complete description of the MFS application to *TS* calculation, including the mathematical description of the complete equations system can be found in Pérez-Arjona *et al.* (2018).

To accurately resolve the acoustic wave the MFS virtual sources were considered and located in a number of at least six sources per wavelength. For the sake of comparison with standard experimental measurements, the simulated emitted acoustic field was assumed to be the corresponding to the analytical solution of the pressure created by a circular piston in its far field (Medwin and Clay, 1998), as an idealization of a scientific echosounder transducer. The transducer size was chosen to produce a half-beam angle at −3 dB of 3.5°, following the specifications of Simrad EK60 scientific echosounders at working frequencies. The MFS model was solved at the three frequencies used for the measurements: 38, 120, and 200 kHz. Moreover, convergence tests were carried out for each frequency to guarantee the proper density mesh. The *TS* directivity was calculated for dorsal incidence with fish tilt angle from $\alpha = -90$ to $\alpha = 90^\circ$ (Figure 5). To study possible fish swimming orientation, an optimization procedure was applied by running the model with tilt angles following sequences of normal distributions. Simulated *TS* values obtained using mean tilt angles from −10° to 10° and standard deviation from −20° to 20° (in increments of 1°) were compared to the experimental *TS*–L relationships, analysing the tilt angles that produced the best agreement.

Results

Near-to-far field experiment

The near-to-far field calibration experiment showed that, when using a gain value obtained by calibrating at the far field, the mean *TS* measured in the far field were the correct nominal *TS* value of the sphere (−42.3 dB). However, the mean *TS* measured at ranges closer than four times the critical range were positively biased by different margins. When using gain values obtained by calibration at each range (Table 4), we were able to measure the same mean unbiased *TS* values of the target at all ranges. This showed that it was possible to correctly measure the *TS* of targets (for example anchovies) in the transition from the near to the far field, by applying calibration values at proper ranges (Figure 6). The gain differences obtained between near-to-far and far field were compared against the analytical solution for the circular piston and were then used to apply the corrections to the *ex situ* anchovy *TS* measurements.

Table 4. Calibration parameters obtained from the *TS* measurements of the sphere in the near-to-far-field (ntff) at 38 kHz.

Depth (m)	*Gain_ntff* (dB)	S_A*Corr_ntff* (dB)
2	22.4	−0.2
3	22.7	−0.2
4	22.4	−0.2
6	22.3	−0.2
12	22.2	−0.2

Power = 800 W, pulse duration = 256 s.

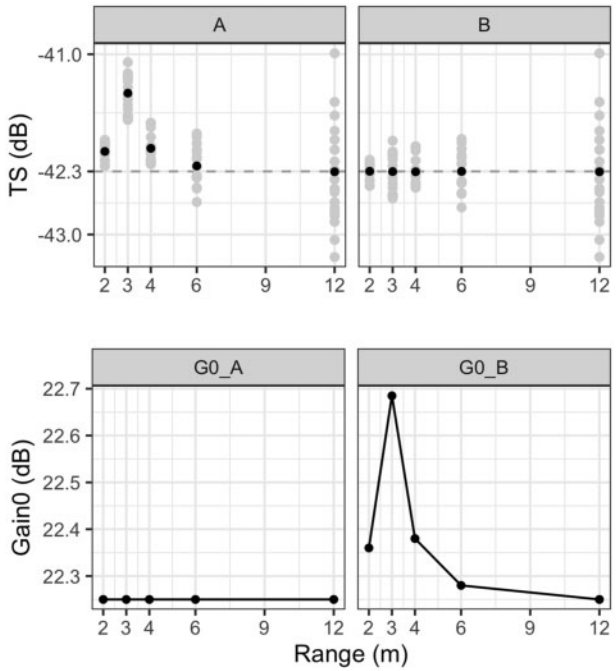

Figure 6. Result of the near-to-far field calibration experiment, using a pulse duration of 256 µs. The upper figure shows a scatterplot (grey circles) of measured *TS* values of the sphere at 38 kHz at different horizontal distances from the transducer face. Black circles mark the mean *TS* value at each range and the grey dotted line, the nominal *TS* value of the tungsten carbide sphere at this frequency (−42.3 dB). (a) The values obtained when using for all distances a single set of calibration parameters obtained at 12 m (i.e. well inside the far field). (b) The measured *TS* values of the sphere using for each distance the calibration parameters obtained at each range (i.e. corrected for the near-to-far field effect). In the figure below, calibrated gain values against range applied in cases a and b are shown.

These calibration results were in general agreement with the analytical solution of a circular flat piston pressure radiation. As explained below, the analytical solution showed an oscillating pattern at the near field, decaying asymptotically at larger distances (Figure 7a). The exact solution and the analytical far field approximation converged at ∼4.5 m from the source (Figure 7a), the deviation between both curves also describing a decreasing pattern with distance (Figure 7b). The comparison of the far vs. near-to-far field deviation between the model and the empirical measurements of the sphere (Figure 7b) showed good agreement for ranges ≥3 m, but the deviation between model prediction and experimental values was important at 2 m. These results pointed to a larger critical range for the 38 kHz transducer than predicted by the model (1.14 m). According to these results, *ex situ TS* measurements of anchovy at depths <2.5 m were discarded at 38 kHz for being less reliable: worse agreement between model and measurements and expected faster *TS* changes with range (Figure 7a). For the rest, we applied bias correction factors according to the interpolated results of the near field experiment.

Measured TS values

Following the plankton filtering (Figure 3), the application of the high-density filter to the *in situ* data retained 30, 52, and 74% of the targets at 38, 12, and 200 kHz, respectively. Concerning *ex situ* measurements, no significant differences were observed among the mean *TS* values measured at different pulse durations (Figure 8). This was intended to be a quality control for the single target detection reliability, thus the lack of differences suggested that the single target detection was correctly achieved at all resolutions. Consequently, all three experiments using the *ex situ* measurement sets were included in the analysis.

Combining both *in situ* and *ex situ* measurements, a total of 6388, 15,695, and 19,012 targets were finally used for the *TS* estimates at 38, 120, and 200 kHz, respectively. The filtered data set covered a depth range of 2.5–27.5 m. The fish length values measured from the different experiments ranged from 3.5 to 19.5 cm, with the highest mean (±standard deviation) value obtained in spring 13.4 (±1.5) cm, and smaller mean values in the cage experiments and autumn survey of 10.4 (±1) and 10 (±3.4) cm, respectively. The highest size variability was observed in the autumn JUVENA survey, with a wider distribution than in the spring BIOMAN survey and cage measurements (Figure 9a) caused by presence in this season of a mixture of juveniles and adults. The filtered *TS* distributions (Figure 9b) were clearly monomodal, except for the 120- and 200-kHz measurements from the cage, where the mode was less pure. Mean *TS* values obtained from the filtered *TS* distributions are presented in Table 5.

TS–length relationships

Overall, the measured *TS* values increased linearly with the logarithm of the fish length. In agreement with the corresponding mean body lengths, the *TS* values were generally higher for the spring hauls than the autumn hauls and the experimental cage results (Figure 9). In sum, the three types of measurements (*ex situ* and *in situ* from both surveys) closely fitted the same *TS* vs. log-length regression. When the slope of the regression was forced to 20, the b_{20} values for the *in situ*-measured data were −66.5, −68.9, and −70.5 dB at 38, 120, and 200 kHz, respectively, and −65.8, −66.4, and −68.7 dB for the *ex situ* measurements (Table 6). When considering the whole data set, these values were −66.4, −68.7, and −70.4 dB. The free-fitting linear model produced significant *in situ* regressions, with slopes of 22.5, 20.5, and 22.5 at the three frequencies, respectively. The non-significant *TS*–L relationship derived from the *ex situ* data was not considered relevant, instead being attributed to the small number of points (only three) available. When considering the entire data set, significant slopes slightly over 20 at the three operative frequencies, with intercepts at −68.7, −69, and −72.9 dB, respectively.

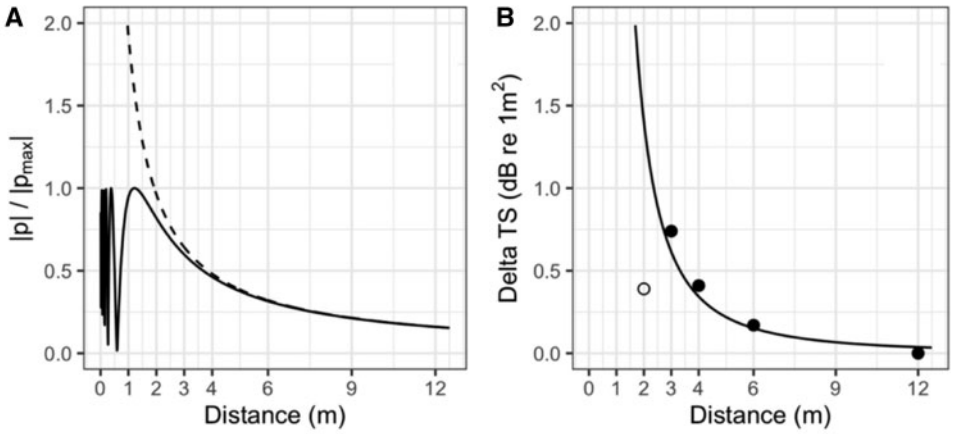

Figure 7. (a) Analytical exact on-axis solution for a circular piston simulating the Simrad ES38B transducer pressure (solid line) and far-field approximation (segmented line) relative to the maximum on-axis radiated pressure (p_{max}) against distance from the source. (b) *TS* deviation between on-axis pressure and far field analytical approximations (solid curve) vs. distance. The circles represent the mean experimental *TS* difference of the sphere between measurements done using near-to-far and far field calibration parameters. Deviation between model prediction and experimental values was important only at 2 m (empty circle).

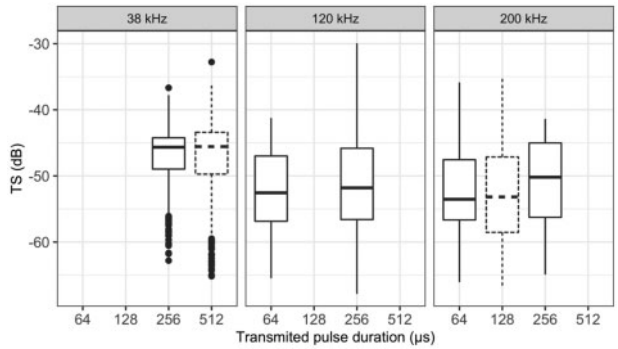

Figure 8. Boxplots summarizing *TS* distributions against pulse duration used in the *ex situ* experiments. Dashed boxplots represent the *TS* distributions of the measurements from set 2, contaminated with 2% of horse mackerel. Pairwise *t*-test produced *p*-values >0.05 within pulse durations considering both contaminated and non-contaminated samples. The boxplots are bounded by first and third quartiles, the central line is the median, and the whiskers show the range of values.

Preliminary linear regression results indicated a *TS* increase with depth at all frequencies (Figure 10), contrarily to expectations of swimbladder compression with pressure increase for a physostomous fish such as anchovy. When building linear models of length against depth, we found a significant ($p < 0.05$ for adults and $p < 0.005$ for juveniles) increase of length also with depth, which, as the *TS* generally increases with fish body length, might explain the unexpected *TS*–depth pattern observed during the night trawls. However, concurrent multiple lineal analyses of *TS* against depth and length were not reliable due to the collinearity found between body length and depth of anchovy. To test whether the unexpected *TS*–depth relationship observed was caused by the increase of length of anchovy, further analyses were conducted: predicted *TS* values were combined with the observed *TS*–length relationship and the expected *TS*–depth relationship from theoretical swimbladder compression following Boylés law (explained in more detail in the corresponding section of the Supplementary material).

Theoretical backscattering of anchovy

The two-chambered swimbladder and backbone simulations (Figure 11) predicted more directive patterns of *TS* vs. swimming tilt angle for increasing frequencies, leading to a steeper reduction in *TS* values with angles for the first ±15°. Thus, although the maximum *TS* values were similar at all frequencies, the mean values were considerably higher for lower frequencies, due to the narrower directivity pattern decreasing the averages when frequency is increased. This agreed with the empirically-measured *TS* frequency response of anchovy at the three experimental frequencies.

The model optimization produced the best values at mean tilt angles of 3 ± 9° (mean value ± standard deviation; $r^2 = 0.9$) for the 38- and 120-kHz frequencies (i.e. swimming slightly oriented downwards). However, at 200 kHz, the best fit was obtained at −5 ± 9° ($r^2 = 0.99$) (slightly oriented upwards (Figure 5)). When considering the three frequencies together, the mean tilt angle was practically 0° (i.e. swimming horizontally). Hence, given the discrepancy observed between the individual fits at the different frequencies (mainly due to the highest directivity of the 200-kHz frequency), a mean tilt angle of 0° was chosen. After fixing the mean tilt value at 0°, the optimization process produced the best standard deviation at 9° for 38- and 120-kHz frequencies ($r^2 = 0.9$); 11° ($r^2 = 0.99$) for 200 kHz; and 10° ($r^2 = 0.9$) when considering the three frequencies together. According to these results, the *a* and *b* values used in the modelled *TS*–L relationships (Figure 12) were obtained considering a compromise "optimum" with a mean tilt angle of 0 ± 10° (Table 6).

The modelled *TS*–L linear regression agreed better with the experimental results at the highest frequency (Table 6). At 38 and 120 kHz, the modelled b_{20} value was 0.7–1 dB lower than the experimental value. At 200 kHz instead, there was practically no difference between the modelled and experimental values.

Discussion

This work presents a comprehensive study of European anchovy *TS* in the Bay of Biscay. A combination of *in situ*, *ex situ* and

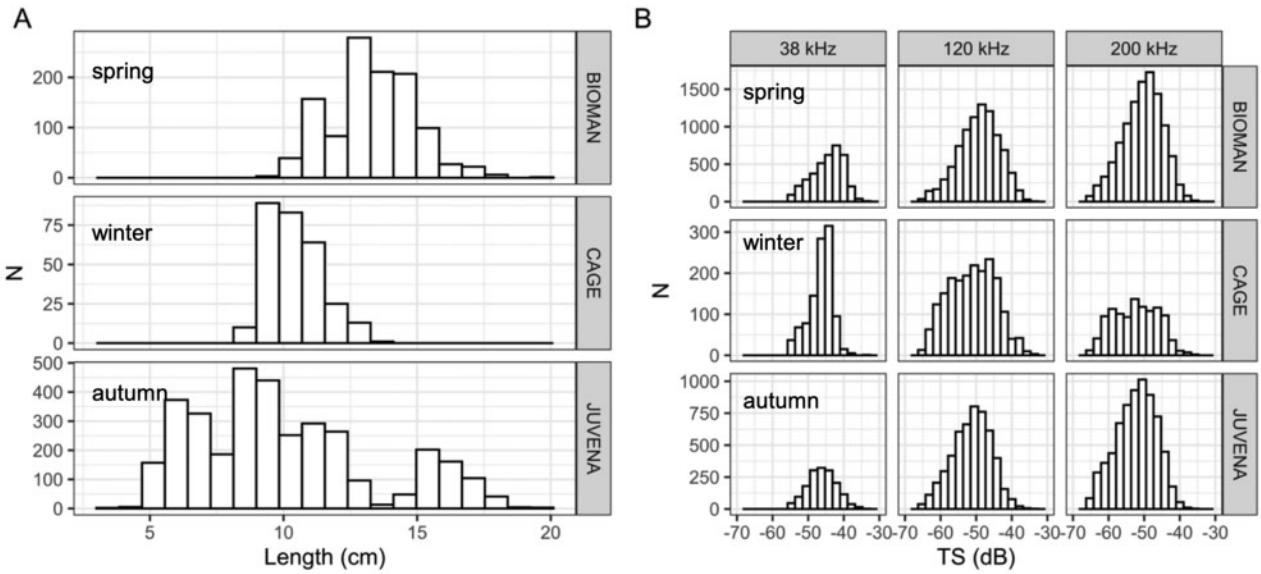

Figure 9. Length (a) and filtered *TS* (b) histograms grouped by *in situ* (BIOMAN, JUVENA) and *ex situ* (cage) measurements.

Table 5. Mean *TS* values (± *SD*) obtained from the filtered *TS* distributions.

	38 kHz	120 kHz	200 kHz
BIOMAN	−43.3(±1.5) dB	−45.4((±2.3) dB	−47.1(±2.1) dB
CAGE	−45.4(±0.9) dB	−45.5(±2.3) dB	−47.7(±2.3) dB
JUVENA	−46.2(±2.7) dB	−49.4(±2.1) dB	−50.3(±2.5) dB

theoretical modelling results are presented of the species-specific *TS*–L relationships to be used for biomass estimation and stock assessment of this species. Data were collected during spring and autumn for 7 years, covering a wide range of fish lengths (3.5–19.5 cm) and physiological conditions. The size and *TS* distributions (Figure 9) at the different sampling periods reflect this seasonality, as the largest specimens were measured during the spring spawning peak (when only adults are present in the area) and the smallest during the autumn survey (when part of the adult stock is absent due to trophic migrations, whereas juveniles predominate) (Boyra *et al.*, 2013). The range of sizes of anchovy used in this experiment practically cover the full range of sizes observed during the acoustic surveys of anchovy in the Bay of Biscay (4–20 cm). The depth range of the anchovies studied (2.5–27.5 m) is in the upper range of the typical 5–120 m of the acoustically sampled depth for assessment (Boyra *et al.*, 2013).

When measuring *TS* values for small pelagic species such as anchovy, two of the key difficulties are to apply a correct lower threshold (Weimer and Ehrenberg, 1975) and to avoid bias by unresolved multiple targets (Soule *et al.*, 1995). The application of an incorrect threshold can affect the lower end of the *TS* distribution by including small targets such as plankton. In the *in situ* measurements, this was avoided by applying a bi-frequency mask to distinguish fish from plankton, as has been successfully demonstrated in other studies (Lezama-Ochoa *et al.*, 2011, 2014; Albaina *et al.*, 2015; Gastauer *et al.*, 2017), whereas in the *ex situ* measurements, this distinction was based on the observed difference between echo-traces according to expected differences in swimming velocity between fish and plankton.

Potential bias due to unresolved multiple echoes was mitigated following different procedures. First, all measurements were made at night to facilitate the detection of single fish targets. Second, the high-density filter (Gauthier and Rose, 2001) applied to the *in situ* measurements further decreased the probability of erroneously assigning to a single fish the echo of multiple targets. As in a previous study (Boyra *et al.*, 2018), the empirically determined N_v value was shown to be independent of the horizontal scale at which it was calculated as well as the initial *TS* value used, thus avoiding the well-known circularity issue of calculating a *TS* value based on a previous one. Finally, the *ex situ* measurement results were similar at different effective resolutions (pulse durations) of the acoustic sensors, supporting the notion that the relatively low fish density at the cage was sufficient to avoid multiple echoes.

An additional difficulty encountered was that a large proportion of the *ex situ* measurements done at 38 kHz were made at distances inside the transition from the near to the far field of the transducer, which, due to the inherent divergence from spherical decay of acoustic beams in this area, were likely to be biased. The *ad hoc* experiment conducted to address this issue was in agreement with predictions by the analytical model of the circular piston (Figure 7b), thereby showing that it is possible to perform unbiased measurements at distances inside the near-to-far field, provided that calibrations are done at those distances. Moreover, the analytical model also showed that we can safely interpolate gain values at intermediate distances, provided that they are farther than the critical range. The observed deviations between the theoretical and empirical location range of critical range (empirical $R_C > 1.14$ m, Figure 7b) can be attributable to an inaccurate knowledge of the specific geometry of the actual transducers. A better knowledge of the construction characteristics of transducers should improve the application of the proposed method. In future studies, this procedure is recommended when making *ex situ* acoustic experiments at short ranges, as it may be helpful to increase the range of valid measurements.

This study has shown significant positive correlations between *TS* and fish length and a good consistency both between *in situ* results from different seasons and between *in situ* and *ex situ*

Table 6. Statistics of the empirical and theoretical (by means of the MFS backscattering model) *TS*–L linear regression parameters.

	Frequency (kHz)	*a*	*B*	b_{20}	*N*
In situ	38	22.2	−68.8	−66.5	53
	120	20.5	−69.5	−68.9	53
	200	22.5	−73.2	−70.5	53
Ex situ	38	–	–	−65.8	3
	120	–	–	−66.4	3
	200	–	–	−68.7	3
In situ + *ex situ*	38	22.2	−68.7 ($r^2 = 0.7$)	**−66.4** ($r^2 = 0.8$)	56
	120	20.2	−69 ($r^2 = 0.7$)	**−68.7** ($r^2 = 0.9$)	56
	200	22.4	−72.9 ($r^2 = 0.5$)	**−70.4** ($r^2 = 0.9$)	56
Theoretical model	38	15.2	−61.8 ($r^2 = 0.9$)	−67.1 ($r^2 = 0.8$)	–
	120	21.6	−71 ($r^2 = 0.9$)	−69.7 ($r^2 = 0.9$)	–
	200	20.2	−70.1 ($r^2 = 1$)	−70.4 ($r^2 = 1$)	–

The number of points available from the *ex situ* measurements was too small, and the length range too narrow to be considered for estimating the *a* and *b* values for *ex situ* data. Results of the whole dataset (including both in situ and ex situ data) in bold.

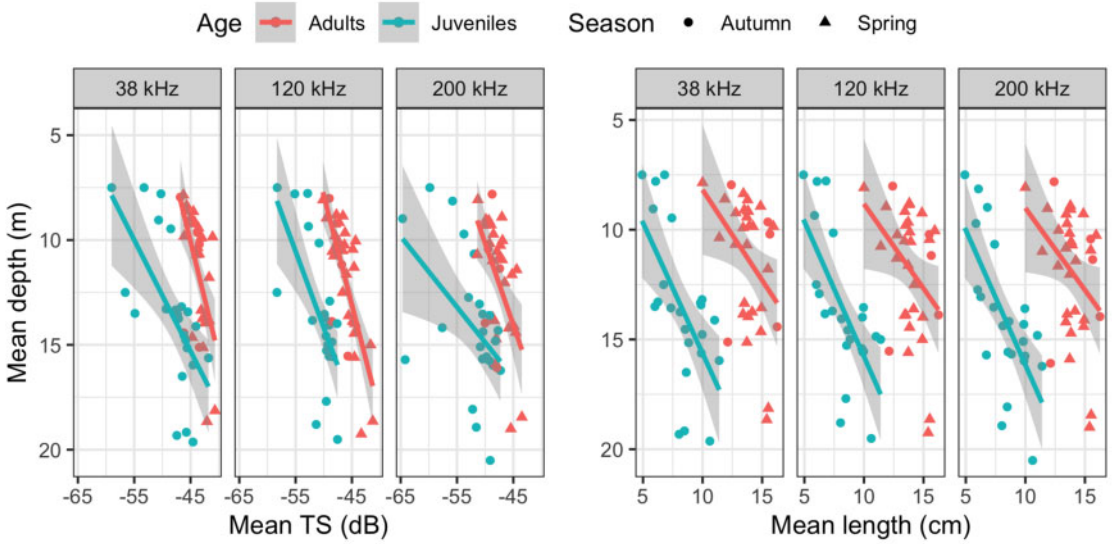

Figure 10. Top panel: relation between anchovy body length and mean depth per haul. Bottom panel: relation between mean *TS* per haul and mean depth. Both graphs distinguish between age groups and seasons.

results. The optimal slope obtained for the whole data set at all frequencies was consistently close to 20, meaning that the horizontal cross-sectional area of the swimbladder changes proportionally to the square of the fish length, as according to expectations (Simmonds and Maclennan, 2005).

Assuming the correct performance of the model and based on the agreement with the experimental results, anchovy swimming orientation tendency should be, on average, not too far from horizontal, but with a rather high variability (standard deviation around 10°). These results should however be taken with care, since the optimization outputs for the different frequencies pointed towards opposite swimming directions, hence making our results not particularly revealing in this matter. Previous studies on similar engraulid species (Aoki and Inagaki, 1988; Madirolas *et al.*, 2016) and other clupeoids (Huse and Ona, 1996) at the night scattering layer described a slightly head up swimming orientation. These results were justified by the need of the fish to compensate a negative buoyancy (Huse and Ona, 1996; Madirolas *et al.*, 2016).

Given that anchovy is a physostomous species and thus unable to compensate its swimbladder volume against pressure changes, it can be expected that *TS* decreases with depth according to Boyle's law, as has been observed in previous measurements of anchovy (Zhao *et al.*, 2008) and other physostomous species (Ona, 2003). In spite of this, we were unable to find evidence of the swimbladder compression on the observed *TS*–length relationship. On the contrary, the unexpected increase of *TS* with depth (Figure 10) was caused by a general depth stratification pattern of anchovies according to body size during night hauls. Our analysis showed that the *TS* increase produced by this length stratification was able (although not completely, Supplementary Figure S1) to justify the observed *TS*–depth increase, prevailing over and masking the expected decrease of *TS* with depth due to swimbladder compression.

The failure to find evidence of swimbladder compression in our *TS*–depth relationships might have owed to the small depth span of our measurements, due to the typical shallower distribution of anchovy at night. An additional factor could be the lack of

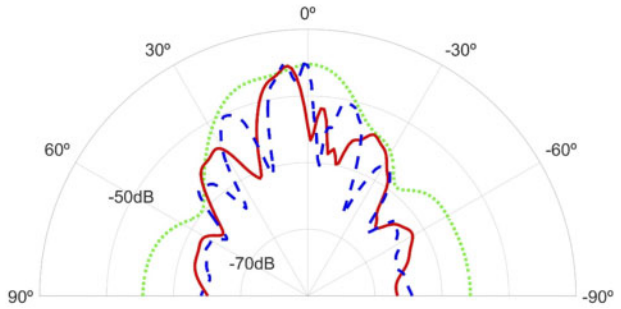

Figure 11. Beam directivity patterns obtained with the backscattering simulation of the two-chambered swimbladder plus backbone at the three frequencies of study. The maximum *TS* values are obtained for a swimming tilt angle of 5° at higher frequencies (120 and 200 kHz), corresponding to more directive *TS* patterns Although these maximum values are similar at all frequencies, the mean *TS* values, for a normal distribution of swimming tilt angles around the horizontal ($\alpha = 0°$), are lower for higher frequencies.

depth resolution of the sampling collection in the *in situ* experiments. The vertical opening of the haul was 15–20 m for near-surface trawls, hence the same magnitude of the whole depth range of the study. Consequently, we might be losing part of the length stratification inside each haul, which would explain the smaller predicted slopes. Other factors that might have yield to such inverted *TS*–depth slope could be for example a higher probability of failure of the single target detection filters with increasing depth or a change of behaviour of anchovy with depth. Consequently, further research is necessary to supplement the measurements obtained in this work at different depth ranges. This is a difficult objective to achieve using echosounders installed on a vessel, because it implies measuring the *TS* during the day, when anchovies operate near the sea bottom (according to their nycthemeral migrations) and aggregate in schools, precluding the identification of single targets. One possible solution would be to use submersible echosounders inside the trawls at different trawl depths to make these measurements.

With respect to the observed increase of anchovy length with depth in night hauls, we consider this an interesting and completely unexpected result in itself. What appears to be happening is that, after the nocturnal migration there occurs a spontaneous stratification of the anchovies by size, perhaps due to change of swimming velocity with body length. Its remarkable to have been able to detect this stratification, given the poor resolution of the pelagic trawl with respect to the full extension of the sampled layer. Therefore, we expect that if this phenomenon is further studied in the future with higher sampling resolution, the observed stratification will be stronger.

Our values lie within the range of the latest published *TS* values obtained for engraulid species. At the most commonly used frequency in fisheries acoustics (38 kHz) (Simmonds and Maclennan, 2005), recent studies have provided $b_{20} = -68.6$ dB on similar species *Engraulis anchoita* (Madirolas *et al.*, 2016), obtained from 11 to 17 cm specimens during night-time *in situ* *TS* measurements. Other experiments on *Engraulis japonicus* (Zhao *et al.*, 2008) have yielded *TS*–length relationships that have predicted *TS* values of −65.8 dB (Kang *et al.*, 2009) for lengths ranging 4.8–12.2 cm and −66.5 dB (Sawada *et al.*, 2009) for 10.6 cm at 70 kHz. The only previous work to have examined the

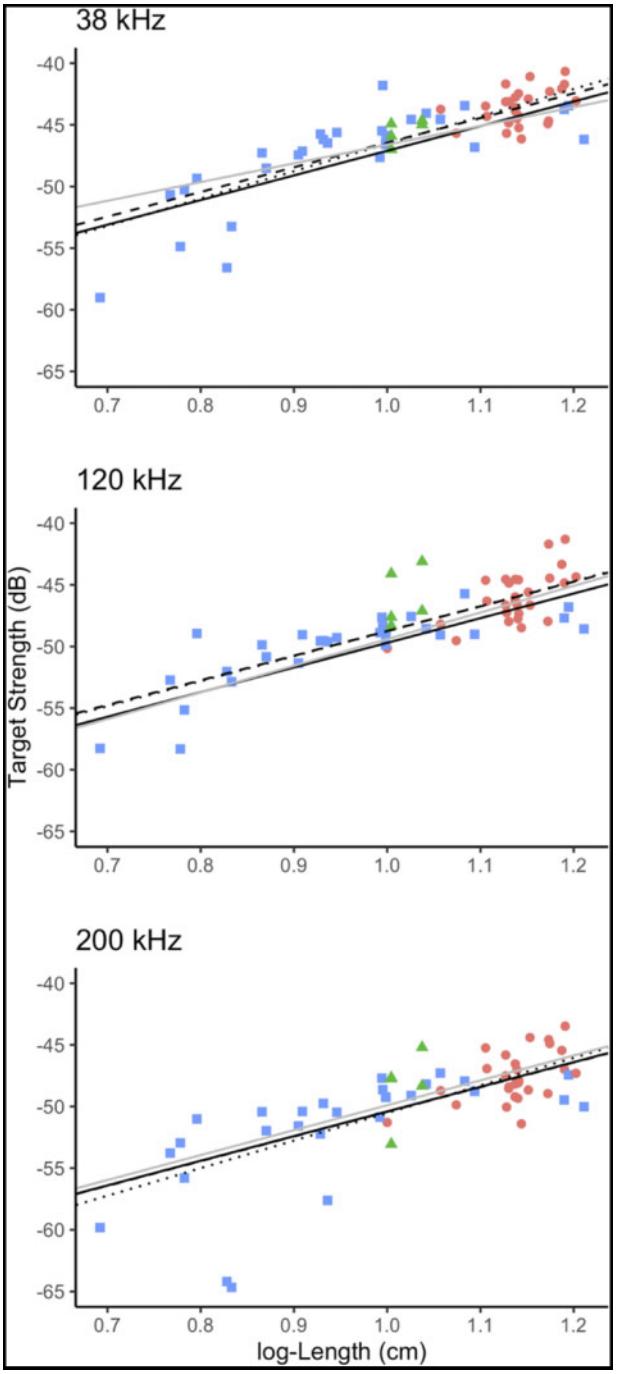

Figure 12. Mean *TS* against total log-length (L) relationship. Dashed line = experimental forced fitting (b_{20}); dotted line = experimental free fitting, bold solid line = theoretical model (b_{20}); and grey solid line = theoretical model free fitting. Red circles correspond to BIOMAN hauls, blue squares to JUVENA hauls, and green triangles to the cage experiments.

TS of European anchovy funnelled the targets through a net with an open cod end, obtaining a b_{20} of −65.2 dB from 12.5-cm anchovies at ∼60-m depth at 70 kHz (Doray *et al.*, 2016). This methodology avoided multiple target bias, but at the expense of forcing the anchovies to swim almost horizontally (i.e. with a narrower distribution of tilt angles than expected to be their natural

behaviour) towards the net mouth. Although the results of that work are not directly comparable with our own due to differences in frequency and behaviour, they can be considered qualitatively consistent. However, these authors predicted a 2-dB decrease at 38 kHz, when increasing the fish tilt angle towards a more "natural" swimming behaviour. Hereby, a b_{20} value of −67.2 dB was reported. This value is consistent with a *TS* reduction with the increased range of tilt angles illustrated in Figure 11.

The obtained *TS* trend with frequency, with higher responses at lower frequencies (Figure 9b), was typical of bladder-bearing fish species (Fernandes *et al.*, 2006). This pattern may prove useful in developing multi-frequency masks to discriminate anchovy from plankton and other pelagic species (Lezama-Ochoa *et al.*, 2011). The backscattering model provided some rough explanation of the *TS* frequency response. According to the model, despite the similarity between the highest *TS* values across frequencies, the greater directivity of the higher frequencies (Figure 11) produced lower mean *TS* values when averaged over a range of tilt angles. In general terms, a rather good general agreement was obtained between the simulations and the empirical results (Table 6).

Implications for assessment

Despite the need for a precise *TS* value in the acoustic assessment of fish abundance, alongside the recommendation that an empirical *TS*–L data relationship be established whenever new data are collected (McClatchie, 2003), biomass estimates of European anchovy in the Bay of Biscay have long been obtained with herring *TS* values published more than three decades ago (ICES, 1982; Degnbol *et al.*, 1985). In response, this study has presented the first *TS* measurements for European anchovy at the frequency of 38 kHz used for assessment. The obtained b_{20} values at 38 kHz were 5–6 dB higher than those currently used by acoustic surveys in the assessment of European anchovy in the Bay of Biscay (Boyra *et al.*, 2013). Such values would represent a more than twofold decrease if applied to estimate the acoustic-based biomass of anchovy.

Nevertheless, the *TS* values were derived at a lower depth ($z \approx 13$ m) than is typical for anchovy during the daytime (i.e. the period at which acoustic surveys are conducted), especially for adults and larger juveniles that are subjected to nycthemeral migrations. Thus, given the expected decrease of *TS* with depth for anchovy and other physostomous species (Ona, 2003; Zhao *et al.*, 2008; Fässler *et al.*, 2009; Madirolas *et al.*, 2016), it is likely that the reduction in acoustic-based biomass will be somewhat lower than that inferred solely from this work. Therefore, it is recommended that further research is conducted to determine the *TS*–depth relationship for anchovy by lowering echosounders at different depths during day and night hauls. The use of this larger depth range should help us avoiding the artefact *TS*–depth relation observed in this work (Figure 10). The findings could then be combined with the present results to produce a thorough *TS*–length–depth relationship to update the acoustic-based assessment of this important species.

Conclusion

This study has provided the first *TS*–length relationship for European anchovy at the frequency used by assessment acoustic surveys (38 kHz) as well as the frequency response at typical frequencies (38, 120, and 200 kHz), which may be useful for building species discrimination masks. The measurements were done targeting anchovies both in their natural environment and in a harbour cage. Special care was taken to reduce the potential bias associated with measuring anchovies *in situ* and to guarantee that *ex situ* measurements are free from bias caused by range. The fact that the linear *TS*–L regressions using the entire *ex situ* and *in situ* data set produced such good fit adds robustness to the estimated values. The values obtained (−66.5, −68.7, and −70.4 dB at 38, 120, and 200 kHz, respectively) are in accordance with recently published values for the *TS* of anchovy in other areas as well as with backscattering models for bladdered fish. This points towards a general overestimation of current acoustic surveys for assessment, although it is necessary to extend the depth range of measurements beyond the ∼13 m of this study before it will be possible to update the assessment of this species in the Bay of Biscay.

Supplementary data

Supplementary material is available at the *ICESJMS* online version of the manuscript.

Acknowledgements

This study was funded by AZTI-Tecnalia and supported by the research projects JAULA for the *ex situ* measurements and JUVENA for the *in situ* ones. The project JAULA was funded by the Department of Agriculture, Fisheries and Food of the Basque Country Government; we thank Unai Cotano, the leader of the project, for giving us access to the cage and for providing biological sampling information. We would like to thank the crew from the Itsas Lagunak for providing us with the anchovy specimens, the Aquaculture School from Mutriku for keeping the specimens during the acclimatization period and the technician and diver Gaizka Bidegain from AZTI for the maintenance and underwater inspection of the specimens used throughout the *ex situ* measurements. Yolanda Lacalle is thanked for the illustration in Figure 2. The project JUVENA was co-funded by the Dirección de Innovación y Desarrollo Tecnológico, Viceconsejería de Política e Industria Alimentaria, Dpto. Agricultura, Pesca y Alimentación of the Basque Government and the Secretaría General del Mar, Ministerio de Agricultura, Alimentación y Medio Ambiente of the Spanish Government. Thanks also to Andrés Uriarte (Azti) for improving this work with his valuable comments and to Mathieu Doray and Laurent Berger (Ifremer) for their helpful suggestions regarding the analysis and the interpretation of the results. Finally, thanks to the anonymous contribution of the reviewers for helping improve the quality and readability of this work.

Author contributions

BS and GB wrote the main manuscript text and were involved in the acquisition, analysis, and interpretation of data. IP-A and VE contributed to the theoretical modelling application and interpretation. UM collected data for the *in situ* analysis. All authors have substantially revised the manuscript.

Data availability

Datasets generated and/or analysed during this study are available from the corresponding author upon reasonable request.

References

Albaina, A., Irigoien, X., Aldalur, U., Boyra, G., Santos, M., and Estonba, A. 2015. Macrozooplankton predation impact on anchovy (Engraulis encrasicolus) eggs mortality at the Bay of Biscay shelf break spawning centre. ICES Journal of Marine Science, 72: 1370–1379.

Andreeva, I. B. 1974. Scattering of sound by air bladders of fish in deep sound-scattering ocean layers. Soviet Physics Acoustics, 10: 17–20.

Aoki, I., and Inagaki, T. 1988. Photographic observations on the behaviour of Japanese anchovy Engraulis japonica at night in the sea. Marine Ecology Progress Series, 43: 213–221.

Ballón, M., Bertrand, A., Lebourges-Dhaussy, A., Gutiérrez, M., Ayón, P., Grados, D., and Gerlotto, F. 2011. Is there enough zooplankton to feed forage fish populations off Peru? An acoustic (positive) answer. Progress in Oceanography, 91: 360–381.

Barange, M., Hampton, I., and Soule, M. 1996. Empirical determination of in situ target strengths of three loosely aggregated pelagic fish species. ICES Journal of Marine Science, 53: 225–232.

Boyra, G., Martínez, U., Cotano, U., Santos, M., Irigoien, X., and Uriarte, A. 2013. Acoustic surveys for juvenile anchovy in the Bay of Biscay: abundance estimate as an indicator of the next year's recruitment and spatial distribution patterns. ICES Journal of Marine Science, 70.

Boyra, G., Moreno, G., Orue, B., Sobradillo, B., and Sancristobal, I. 2019. In situ target strength of bigeye tuna (*Thunnus obesus*) associated with fish aggregating devices. ICES Journal of Marine Science, 76: 2446–2458.

Boyra, G., Moreno, G., Sobradillo, B., Pérez-Arjona, I., Sancristobal, I., and Demer, D. A. 2018. and Handling editor: purnima Ratilal Target strength of skipjack tuna (Katsuwanus pelamis) associated with fish aggregating devices (FADs). ICES Journal of Marine Science, 75: 1790–1802.

Chu, D., and Eastland, G. C. 2015. Calibration of a broadband acoustic transducer with a standard spherical target in the near field. The Journal of the Acoustical Society of America, 137: 2148–2157.

Degnbol, P., Lassen, H., and Staehr, K. J. 1985. In-situ determination of target strength of herring and sprat at 38 and 120 kHz. Dana, 5: 45–54.

Demer, D. a., Berger, L., Bernasconi, M., Bethke, E., Boswell, K. M., Chu, D., Domokos, R., *et al.* 2015. Calibration of acoustic instruments. ICES Cooperative Research Report, 326: 133.

Doray, M., Berger, L., Le Bouffant, N., Coail, J. Y., Vacherot, J. P., de La Bernardie, X., Morinière, P., *et al.* 2016. A method for controlled target strength measurements of pelagic fish, with application to European anchovy (*Engraulis encrasicolus*). ICES Journal of Marine Science, 73: 1987–1997.

Echoview Software. 2013. Echoview Software Pty Lt, Hobart, Tasmania, Australia.

Fairweather, G., Karageorghis, A., and Martin, P. A. 2003. The method of fundamental solutions for scattering and radiation problems. Engineering Analysis with Boundary Elements, 27: 759–769.

Fässler, S. M. M., Fernandes, P. G., Semple, S. I. K., and Brierley, A. S. 2009. Depth-dependent swimbladder compression in herring Clupea harengus observed using magnetic resonance imaging. Journal of Fish Biology, 74: 296–303.

Fernandes, A., Masse, J., Iglesias, M., Diner, N., and Ona, E. 2006. The SIMFAMI Project: Species Identification Methods from Acoustic Multi-Frequency Information. Aberdeen, UK. Final Report to the EC Number Q5RS-2001-02054, 486 pp.

Fernandes, P. G., Copland, P., Garcia, R., Nicosevici, T., and Scoulding, B. 2016. Additional evidence for fisheries acoustics: small cameras and angling gear provide tilt angle distributions and other relevant data for mackerel surveys. ICES Journal of Marine Science, 73: 2009–2019.

Foote, K. G. 2014. Discriminating between the nearfield and the farfield of acoustic transducers. The Journal of the Acoustical Society of America, 136: 1511–1517.

Foote, K. G. 1980. Importance of the swimbladder in acoustic scattering by fish: a comparison of Gadoid and mackerel target strengths. The Journal of the Acoustical Society of America, 67: 2084–2089.

Foote, K. G., and Francis, D. T. 2002. Comparing Kirchhoff-approximation and boundary-element models for computing gadoid target strengths. The Journal of the Acoustical Society of America, 111: 1644–1654.

Foote, K. G., Knudsen, H. P., Vestnes, G., MacLennan, D. N., and Simmonds, E. J. 1987. Calibraton of acoustic instruments for fish density estimation: a practical guide. ICES Cooperative Research Report 144. Copenhagen.

Fujino, T., Sadayasu, K., Abe, K., Kidokoro, H., Tian, Y., Yasuma, H., and Miyashita, K. 2009. Swimbladder morphology and target strength of a mesopelagic fish, Maurolicus japonicus. Journal of Marine Acoustics Society of Japan, 36: 241–249.

Furusawa, M. 1988. Prolate spheroidal models for predicting general trends of fish target strength. Journal of the Acoustic Society of Japan, 9: 13–24.

Gastauer, S., Scoulding, B., and Parsons, M. 2017. Estimates of variability of goldband snapper target strength and biomass in three fishing regions within the Northern Demersal Scalefish Fishery (Western Australia). Fisheries Research, 193: 250–262.

Gauthier, S., and Rose, G. A. 2001. Diagnostic tools for unbiased in situ target strength estimation. Canadian Journal of Fisheries and Aquatic Sciences, 58: 2149–2155.

Glass, C. 2000. Dynamics of Pelagic Fish Distribution and Behaviour: Effects on Fisheries and Stock Assessment. Pierre Fréeon and Ole Arve Misund. Reviews in Fish Biology and Fisheries, 10: 124–124.

Godinho, L. M. C., Costa, E., Pereira, A., and Santiago, J. 2012. Some observations on the behaviour of the method of fundamental solutions in 3D acoustic problems. International Journal of Computational Methods, 09: 04: 1250049.

Gorska, N., Ona, E., and Korneliussen, R. 2005. Acoustic backscattering by Atlantic mackerel as being representative of fish that lack a swimbladder. Backscattering by individual fish. ICES Journal of Marine Science, 62: 984–995.

Henderson, M. J., and Horne, J. K. 2007. Comparison of in situ, ex situ, and backscatter model estimates of Pacific hake (Merluccius productus) target strength. Canadian Journal of Fisheries and Aquatic Sciences, 64: 1781–1794.

Huse, I., and Ona, E. 1996. Tilt angle distribution and swimming speed of overwintering Norwegian spring spawning herring. ICES Journal of Marine Science, 53: 863–873.

Ibaibarriaga, L., Fernández, C., Uriarte, A., and Roel, B. A. 2008. A two-stage biomass dynamic model for Bay of Biscay anchovy: a Bayesian approach. ICES Journal of Marine Science, 65: 191–205.

ICES. 1982. Report of the 1982 Planning Group on ICES-Coordinated Herring and Sprat Acoustic Surveys. ICES Document CM 1982/H: 04.

ICES. 2013. ICES WGACEGG REPORT 2013 Working Group on Acoustic and Egg Surveys for Sardine and Anchovy in ICES Areas VIII and IX (WGACEGG) By Correspondence and 25–29 November 2013. ICES CM, SSGESST:20. 131 pp.

ICES. 2015. Report of the Working Group on Southern Horse Mackerel, Anchovy and Sardine (WGHANSA). ICES CM, ACOM: 16. 580 pp.

ICES. 2017. Report of the Working Group on Southern Horse Mackerel, Anchovy and Sardine (WGHANSA), 24–29 June 2017, Bilbao, Spain.

Jech, J. M., and Horne, J. K. 2001. Effects of in situ target spatial distributions on acoustic density estimates. ICES Journal of Marine Science, 58: 123–136.

Jech, J. M., Horne, J. K., Chu, D., Demer, D. A., Francis, D. T. I., Gorska, N., Jones, B., *et al.* 2015. Comparisons among ten models

of acoustic backscattering used in aquatic ecosystem research. The Journal of the Acoustical Society of America, 138: 3742–3764.

Kang, D., Cho, S., Lee, C., Myoung, J.-G., and Na, J. 2009. Ex situ target-strength measurements of Japanese anchovy (Engraulis japonicus) in the coastal Northwest Pacific. ICES Journal of Marine Science, 66: 1219–1224.

Kang, D., and Hwang, D. 2003. Ex situ target strength of rockfish (Sebastes schlegeli) and red sea bream (Pagrus major) in the Northwest Pacific. ICES Journal of Marine Science, 60: 538–543.

Kieser, R., Mulligan, T. and Ehrenberg, J. 2000. Observation and explanation of systematic split-beam angle measurement errors. Aquat. Living Resour. 7.

Kinsler, L. E., Frey, A. R., Coppens, A. B., and Sanders, J. V. 1999. Fundamentals of acoustics. *In* Fundamentals of Acoustics, 4th edn, p. 560. Ed. by L. E. Kinsler, A. R. Frey, A. B. Coppens, and J V. Sanders. ISBN: 0-471-84789-5. Wiley-VCH, USA.

Lezama-Ochoa, A., Ballón, M., Woillez, M., Grados, D., Irigoien, X., and Bertrand, A. 2011. Spatial patterns and scale-dependent relationships between macrozooplankton and fish in the Bay of Biscay: an acoustic study. Marine Ecology Progress Series, 439: 151–168.

Lezama-Ochoa, A., Irigoien, X., Chaigneau, A., Quiroz, Z., Lebourges-Dhaussy, A., and Bertrand, A. 2014. Acoustics reveals the presence of a macrozooplankton biocline in the Bay of Biscay in response to hydrological conditions and predator-prey relationships. PLoS One, 9: e88054.

Lilja, J., Marjomäki, T. J., Jurvelius, J., Rossi, T., and Heikkola, E. 2004. Simulation and experimental measurement of side-aspect target strength of Atlantic salmon (Salmo salar) at high frequency. Canadian Journal of Fisheries and Aquatic Sciences, 61: 2227–2236.

Love, R. H. 1977. Target strength of an individual fish at any aspect. The Journal of the Acoustical Society of America, 62: 1397.

Love, R. H. 1978. Resonant acoustic scattering by swimbladder-bearing fish. The Journal of the Acoustical Society of America, 64: 571–580.

MacLennan, D., Armstrong, F., and Simmonds, E. 1990. Further observations on the attenuation of sound by aggregations of fish. Proceedings of the Institute of Acoustics (UK), 12: 99–106.

Maclennan, D. N., Fernandes, P. G., and Dalen, J. 2002. A consistent approach to definitions and symbols in fisheries acoustics. ICES Journal of Marine Science, 59: 365–369.

Madirolas, A., Membiela, F. a., Gonzalez, J. D., Cabreira, A. G., dell'Erba, M., Prario, I. S., and Blanc, S. 2016. Acoustic target strength (TS) of argentine anchovy (*Engraulis anchoita*): the nighttime scattering layer. ICES Journal of Marine Science, 74: 1408–1420.

Massé, J., Duhamel, E., Petitgas, P., Doray, M., and Huret, M. 2018. Pelagic Survey Series for Sardine and Anchovy in ICES Subareas 8 and 9—Towards an Ecosystem Approach. Ed. by J. Massé, A. Uriarte, M. Manuel Angélico, and P. Carrera. http://www.ices.dk/sites/pub/Publication%20Reports/Cooperative%20Research%20Report%20(CRR)/CRR%20332.pdf (last accessed 29 October 2019).

McClatchie, S., Macaulay, G. J., and Coombs, R. F. 2003. A requiem for the use of 20log10Length for acoustic target strength with special reference to deep-sea fishes. ICES Journal of Marine Science, 60: 419–428.

Medwin, H., and Clay, C. S. 1998. Fundamentals of Acoustical Oceanography. Applications of Modern Acoustics. Academic Press, Boston. 712 pp.

Murase, H., Kawabata, A., Kubota, H., Nakagami, M., Amakasu, K., Abe, K., and Miyashita, K. 2011. Effect of depth-dependent target strength on biomass estimation of japanese anchovy. Journal of Marine Science and Technology, 19: 267–272.

Ona, E., and Barange, M. 1999. Single target recognition. CRR, Methodology for Target Strength Measurement, 235. http://www.ices.dk/sites/pub/Publication%20Reports/Cooperative%20Research%20Report%20(CRR)/crr235/CRR235.pdf (last accessed 28 February 2017).

Ona, E. 2003. An expanded target-strength relationship for herring. ICES Journal of Marine Science, 60: 493–499.

Peltonen, H., and Balk, H. 2005. The acoustic target strength of herring (Clupea harengus L.) in the northern Baltic Sea. ICES Journal of Marine Science, 62: 803–808.

Pérez-Arjona, I., Godinho, L., and Espinosa, V. 2018. Numerical simulation of target strength measurements from near to far field of fish using the method of fundamental solutions. Acta Acustica United with Acustica, 104: 25–38.

Pérez-Arjona, I., Godinho, L. M. C., and Espinosa, V. 2020a. Numerical simulation of target strength measurements from near to far field of fish using the method of fundamental solutions. ICES Journal of Marine Science.

Pérez-Arjona, I., Godinho, L., and Espinosa, V. 2020b. Influence of fish backbone model geometrical features on the numerical target strength of swimbladdered fish. ICES Journal of Marine Science.

Santos, M., Uriarte, A., Boyra, G. and Ibaibarriaga, L. 2016. Anchovy DEPM Surveys 2003-2012 in the Bay of Biscay (Subarea VIII) BIOMAN. ICES Cooperative Research Report, Pelagic Surveys Series for Sardine and Anchovy in ICES Areas VIII and IX (WGACEGG), 332. International Council for the Exploration of the Sea (ICES), Copenhagen.

Sawada, K., Furusawa, M., and Williamson, N. J. 1993. Conditions for the precise measurement of fish target strength in situ. The Journal of the Marine Acoustics Society of Japan, 20: 73–79.

Sawada, K., Takahashi, H., Abe, K., Ichii, T., Watanabe, K., and Takao, Y. 2009. Target-strength, length, and tilt-angle measurements of Pacific saury (Cololabis saira) and Japanese anchovy (Engraulis japonicus) using an acoustic-optical system. ICES Journal of Marine Science, 66: 1212–1218.

Sawada, K., Uchikawa, K., Matsuura, T., Sugisaki, H., and Amakasu, K., Abe, K. 2011. In situ and ex situ target strength measurement of mesopelagic lanternfish, Diaphus Theta (Family Myctophidae). Journal of Marine Science and Technology, 19: 302–311.

Simmonds, J. E., and Maclennan, D. N. 2005. Fisheries Acoustics Theory and Practice. 2nd edn. Chapman & Hall, New York. 472 pp.

Soule, M., Barange, M., and Hampton, I. 1995. Evidence of bias in estimates of target strength obtained with a split-beam echo-sounder. ICES Journal of Marine Science, 52: 139–144.

Soule, M. 1997. Performance of a new phase algorithm for discriminating between single and overlapping echoes in a split-beam echosounder. ICES Journal of Marine Science, 54: 934–938.

Torgersen, T., and Kaartvedt, S. 2001. In situ swimming behaviour of individual mesopelagic fish studied by split-beam echo target tracking. ICES Journal of Marine Science, 58: 346–354.

Weimer, R., and Ehrenberg, J. 1975. Analysis of threshold-induced bias inherent in acoustic scattering cross-section estimates of individual fish. Journal of the Fisheries Board of Canada, 32: 2547–2551.

Weston, D. E. 1966. Sound propagation in the presence of bladder fish. In Underwater Acoustics, pp. 55–58. Ed. by V. M. Albers. Plenum, New York.

Ye, Z. 1997. Low-frequency acoustic scattering by gas-filled prolate spheroids in liquids. The Journal of the Acoustical Society of America, 101: 1945–1952.

Zare, P., Kasatkina, S. M., Shibaev, S. V., and Fazli, H. 2017. In situ acoustic target strength of anchovy kilka (Clupeonella engrauliformis) in the Caspian Sea (Iran). Fisheries Research, 186: 311–318.

Zhao, X., Wang, Y., and Dai, F. 2008. Depth-dependent target strength of anchovy (Engraulis japonicus) measured in situ. ICES Journal of Marine Science, 65: 882–888.

Handling editor: Richard O'Driscoll